PROCEEDINGS OF SCIENCE

TTK-24-52

Electric dipole moments: a gateway to new physics

Andrea Shindler[a,b,c,*]

[a] *Institute for Theoretical Particle Physics and Cosmology, TTK, RWTH Aachen University*
[b] *Nuclear Science Division, Lawrence Berkeley National Laboratory, Berkeley, CA 94720, USA*
[c] *Department of Physics, University of California, Berkeley, CA 94720, USA*

E-mail: shindler@physik.rwth-aachen.de

The observed baryon asymmetry in the universe cannot be reconciled with the current form of the Standard Model (SM) of particle physics. The amount of CP-violation stemming from the Cabibbo-Kobayashi-Maskawa matrix is not sufficient to explain the observed matter-antimatter asymmetry. The electric dipole moment (EDM) of the neutron offers a unique opportunity to discover physics beyond the SM (BSM) due to its significantly suppressed CP-violating contribution from the SM. After a brief summary of the current status for experimental searches of a neutron EDM, I introduce the various sources of CP-violation and the computational challenges associated with calculating the corresponding hadronic matrix elements using the lattice as a regulator of QCD. I then describe recent calculations of the nucleon EDM induced by the theta term and recent progress on the calculation of the BSM contributions to the EDM. The numerical and theoretical developments of the last few years are paving the way to a new generation of lattice QCD computation that will provide invaluable information when the next generation of EDM searches will produce their first results.

European network for Particle physics, Lattice field theory and Extreme computing (EuroPLEx2023)
11-15 September 2023
Berlin, Germany

*Speaker

PoS(EuroPLEx2023)024

1. Matter-antimatter asymmetry

The symmetry of masses and decay rates between particles and their antiparticles is a fundamental result of the CPT invariance theorem. However, contrary to expectations of equal particle and antiparticle densities, observations reveal a stark dominance of matter over antimatter in the Universe. A useful parameter to describe this asymmetry is $\eta = \frac{n_B}{n_\gamma}$ with $n_B = n_b - n_{\overline{b}}$, where n_b and $n_{\overline{b}}$ denote the densities of baryons and antibaryons, respectively, and n_γ represents the photon density.

The parameter η can be determined by comparing the observed and predicted abundances of light elements under the standard Big Bang Nucleosynthesis (BBN) model. Assuming a fixed neutrino count, BBN predicts the relative abundances of D, ^{3}He, ^{4}He, and ^{7}Li as functions of η. Experimental measurements of these abundances allow for the inference of η. Figure 1 illustrates these predictions with 95% confidence level bands [1]. Recent analyses incorporating Planck data are discussed in Ref. [2].

Excluding lithium abundance[1], the values of η obtained from D and ^{4}He abundances are consistent. Based on recent D/H abundance measurements [3], η is constrained to $5.8 \times 10^{-10} < \eta < 6.3 \times 10^{-10}$ [1, 2].

An independent determination of η comes from measurements of the Cosmic Microwave Background (CMB) angular power spectrum [4]. The latest Planck data analysis reports $\eta = (6.12 \pm 0.04) \times 10^{-10}$ [5], which agrees well with the BBN-based values.

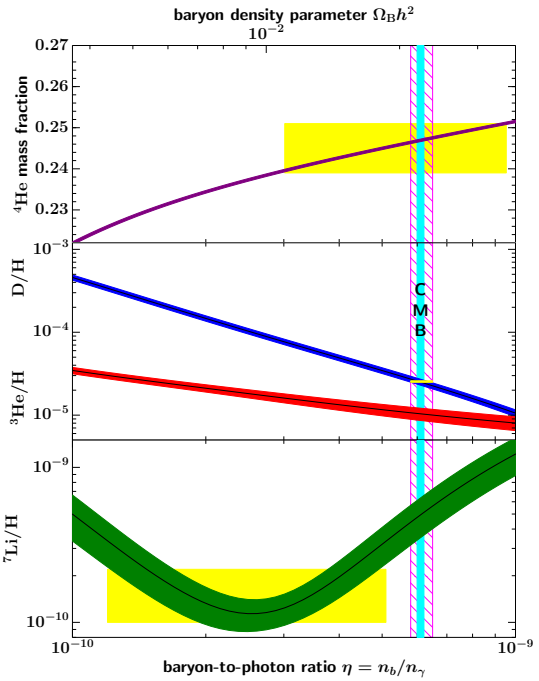

Figure 1: Predicted primordial abundances of light nuclei, including ^{4}He, D, ^{3}He, and ^{7}Li, as functions of the baryon-to-photon ratio η according to standard Big-Bang nucleosynthesis (BBN). Shaded bands show 95% confidence levels. Experimental results are in yellow, while vertical bands indicate the CMB-inferred baryon density (narrow band) and the concordance range for BBN predictions (wider band). Figure taken from Ref. [1].

Irrespective of the underlying particle physics mechanism for baryon asymmetry, three key conditions, known as the Sakharov criteria [6], must be fulfilled: violation of baryon number conservation, C- and CP-symmetry breaking, and a departure from thermal equilibrium to prevent the asymmetry from being erased by thermal averaging.

The CP-violation in the Standard Model (SM) originating from the Cabibbo-Kobayashi-Maskawa (CKM) matrix [7, 8], involving a product of mixing angles, results in an effect as small as 10^{-20}[9–11], which is insufficient to account for the baryon asymmetry observed in the

[1]The mismatch in η values derived from lithium abundance compared to other elements is known as the *lithium problem*.

Universe. This limitation has led to significant interest in baryogenesis mechanisms beyond the Standard Model (BSM)[12].

2. Electric dipole moments and new physics

The intrinsic electric dipole moment (EDM) **d** of a system, as dictated by the Wigner-Eckart theorem, must be aligned with its angular momentum, $\mathbf{d} = d\,\langle \mathbf{J} \rangle$. For a spin-1/2 particle described by the field ψ interacting with the electromagnetic field $F_{\mu\nu}$, the Lagrangian in Minkowski space is given by [13]

$$\mathcal{L} = -\mu\bar{\psi}\sigma^{\mu\nu}F_{\mu\nu}\psi - id\bar{\psi}\gamma_5\sigma^{\mu\nu}F_{\mu\nu}\psi,, \tag{1}$$

where μ represents the magnetic moment. The second term in Eq. (1), associated with the EDM, d, explicitly breaks parity (P) and time-reversal (T) symmetries.

The intrinsic EDM serves as a fundamental probe for uncovering CP-violation, regardless of whether its origin lies within the SM or comes from BSM physics, with potential links to the baryon asymmetry of the Universe. This task necessitates probing EDMs across various systems together with significant theoretical advancements. The ability to detect new physics through EDM searches depends on improving experimental sensitivity across multiple systems, as different sources of CP violation may produce distinct hierarchies and patterns of EDMs. The reach of EDM experiments can be estimated by the energy scale they probe under the assumption of maximal CP violation. Current estimates suggest that EDMs are sensitive to extremely high energy scales, venturing into unexplored domains of physics [14]. If instead new physics is situated near the electroweak scale, EDM measurements remain invaluable by probing minuscule CP-violating couplings.

2.1 The neutron electric dipole moment

The global effort to measure the neutron electric dipole moment (nEDM) has made significant progress, with multiple experiments underway. The PSI collaboration has implemented key improvements, and in 2020, published a new nEDM measurement of $(0.0 \pm 1.1_{\text{stat}} \pm 0.2_{\text{sys}}) \times 10^{-26}\ e \cdot$ cm [15], achieving a fivefold reduction in systematic errors along with moderate statistical gains. Their next-generation n2EDM apparatus, featuring a double-chamber spin precession design first implemented by the PNPI experiment [16], is currently under development. Other major efforts include the double-chamber nEDM experiment at PNPI using the ILL turbine source [16], the panEDM experiment utilizing the SuperSUN source at ILL [17], the TUCAN experiment employing the TRIUMF superfluid helium UCN source [18], and the LANL nEDM experiment [19]. Over the next decade, experimental advancements aim to improve the current nEDM sensitivity by one to two orders of magnitude, as shown by the steady progress in Fig. 2 (see Ref. [14] for a recent summary).

3. CP-violating sources and role of lattice QCD

The SM provides two sources of CP violation: the CKM matrix phase and the θ term in the QCD Lagrangian. The CKM matrix contributes to quark EDMs through a two-loop process [20, 21]. For the nEDM, the leading CKM contribution originates from a $\Delta S = 1$ CP-violating penguin diagram

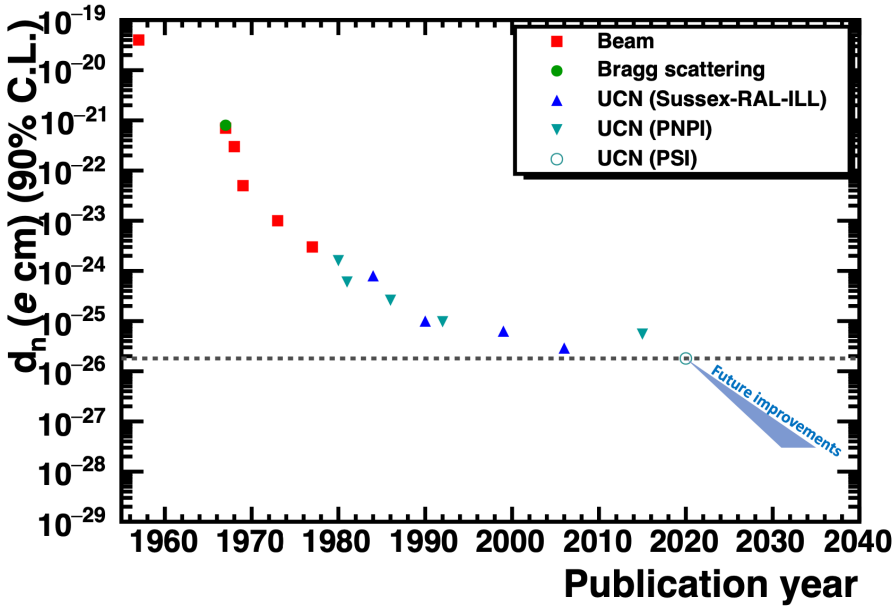

Figure 2: Temporal progression of neutron EDM measurements and anticipated sensitivity improvements. Figure taken from Ref. [14].

(Fig. 3, left). This CP-violating interaction combines with a CP-conserving $\Delta S = 1$ process via a one-loop mechanism, with an enhancement from chiral logarithms (Fig. 3, right).

Recent estimates place the CKM-induced nEDM at $d_n^{\rm CKM} = 1 - 6 \times 10^{-32}$ e cm [22], with uncertainties arising from hadronic effects. This value is approximately six orders of magnitude below the current experimental sensitivity (see Sec. 2.1). As a result, any near-future measurement of the nEDM would provide a definitive signal of new BSM physics.

The flavor-diagonal CP-odd θ term offers a natural source of CP violation. In Minkowski space, the QCD Lagrangian with the θ term for $N_f = 3$ quark flavors and a diagonal mass matrix M is expressed as:

$$\mathcal{L}_{\rm QCD+\bar\theta} = -\frac{1}{4} G^a_{\mu\nu} G^{a,\mu\nu} + \bar\psi (i \not{D} - M)\psi - \bar\theta \frac{g^2}{64\pi^2} \epsilon^{\mu\nu\alpha\beta} G^a_{\mu\nu} G^a_{\alpha\beta} \ , \tag{2}$$

where D_μ is the covariant derivative, $\psi = (u, d, s)^T$ represents the quark fields, and $G^a_{\mu\nu}$ denotes the gluon field tensor. Here, $\epsilon^{0123} = +1$ is the fully antisymmetric tensor, and the CP-violating operator, known as the θ term, is proportional to the coupling $\bar\theta$.

The parameter $\bar\theta$ depends on the chosen basis, with the quark mass matrix made real by absorbing its complex phase into a redefined coupling $\bar\theta = \theta + \arg\det(M)$. This basis aligns with lattice QCD (LQCD) calculations, where the θ term corresponds to a CP-violating pure gauge operator.

Beyond the θ term in the QCD Lagrangian, new CP-violating effects can arise from a general BSM theory introducing heavy particles at a scale $\Lambda_{\rm BSM}$. Below this scale, the effects of these heavy states can be described by effective local operators constructed from SM fields. Operators not present in the SM appear as higher-dimensional terms suppressed by powers of $1/\Lambda_{\rm BSM}^{D-4}$, where D is the operator's dimension. For a detailed discussion of CP-violating operators, see Ref. [23].

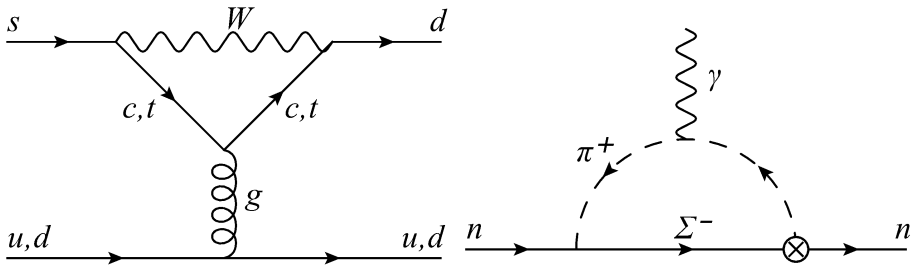

Figure 3: Left: A CP-violating $\Delta S = 1$ penguin diagram. Right: The CP-violating $\Delta S = 1$ operator interacts with a CP-conserving $\Delta S = 1$ coupling. The crossed circle indicates the effective $\not{C}\not{P}$ operator derived from the penguin diagram on the left, contributing to the CKM-induced neutron EDM.

Focusing on dimension-6 operators, the effective Lagrangian is:

$$\mathcal{L}^{\text{eff}}_{\text{BSM}} = \frac{1}{\Lambda^2_{\text{BSM}}} \sum_i C_i^{(6)} O_i^{(6)}, \tag{3}$$

where $C_i^{(6)}$ are Wilson coefficients and $O_i^{(6)}$ are the corresponding operators. After electroweak symmetry breaking, the Higgs field is replaced by its vacuum expectation value, resulting in operators amenable to lattice QCD (LQCD) calculations.

Key operators contributing to the EDM include the quark-chromo EDM (qCEDM), the CP-violating three-gluon operator (also known as the gluon-chromo EDM, or gCEDM), and specific four-fermion operators. The qCEDM operator is given by:

$$O_{\text{qC}}(x) = -i \sum_f \overline{\psi}_f(x) \gamma_5 \sigma^{\mu\nu} G_{\mu\nu} \psi_f(x), \tag{4}$$

where $G_{\mu\nu}$ is the gluon field tensor and ψ_f represents the quark field of flavor f. The gCEDM operator is expressed as:

$$O_{\text{gC}}(x) = \frac{1}{3} f^{ABC} \widetilde{G}^{A,\mu\nu} G^B_{\mu\rho} G^{C,\rho}_{\nu}, \tag{5}$$

where $\widetilde{G}_{\mu\nu} = 1/2 \varepsilon_{\mu\nu\alpha\beta} G^{\alpha\beta}$ is the dual gluon field tensor. Four-fermion operators are categorized into semi-leptonic (containing two quark and two lepton fields) and purely hadronic (four-quark) types, though no lattice QCD results for these operators exist at present.

The role of LQCD calculations is to provide renormalized hadronic matrix elements of CP-violating operators. These matrix elements are critical inputs for disentangling and constraining contributions to any experimentally observed EDM. The nucleon EDM, incorporating contributions from both the θ term and BSM sources, can be parametrized as:

$$d_{\text{N}} = M^{\theta}_{\text{N}} \bar{\theta} + \left(\frac{v}{\Lambda_{\text{BSM}}} \right)^2 \sum_i M^{(i)}_{\text{N}} \widetilde{d}_i, \tag{6}$$

where M^{θ}_{N} and $M^{(i)}_{\text{N}}$ are the LQCD-calculated matrix elements for the θ term and dimension-6 operators, respectively. Here, $\widetilde{d}_i$ represents contributions from Wilson coefficients, and v is the Higgs vacuum expectation value. Perturbative methods determine $\widetilde{d}_i$, while non-perturbative techniques focus on $M^{(i,\theta)}_{\text{N}}$. The importance of a LQCD calculation can be exemplified using the

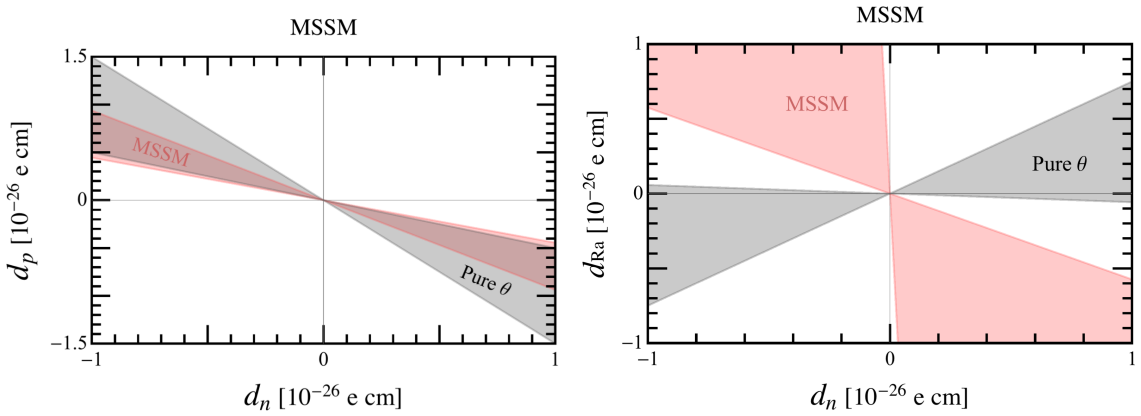

Figure 4: Left: correlation between the neutron EDM and the proton EDM assuming that only the θ term contributes (gray), and the MSSM (red), dominated by the qCEDM operator at hadronic scales. The width of the bands indicate the uncertainty in the ratios arising from hadronic matrix elements. Right: same as left plot for the neutron EDM and the ^{225}Ra EDM. Plots taken from Ref. [24].

phenomenological analysis of Ref. [24], where the impact of the uncertainty in the theoretical EDM estimate has been correlated between several systems and several CP-violating sources. The plots of Fig. 4 show the correlation between the nEDM and the proton EDM (left plot) and the ^{225}Ra EDM (right plot). The grey band represents the scenario in which the θ term is the solely source of CP-violation while the red band represents the correlation from a minimal supersymmetric model (MSSM) where the dominant contribution comes from the qCEDM operator. In the case of the neutron and proton systems becomes critical to reduce the uncertainy of the hadronic matrix element which is responsible for the width of the grey band. Only in this case experimental measurements could actually provide information on the source of CP-violation. Analogously the LQCD community should start delivering a precise determination for the qCEDM in the nucleon system, while the width of the red band is currently given by the uncertainty estimated from QCD sum rules determinations [24]. For a review of recent lattice QCD results on EDMs, see Ref. [25].

4. Electric dipole moment form lattice QCD

To determine the EDM of a nucleon N, it is necessary to evaluate the hadronic matrix element in a CP-violating vacuum

$$\left\langle N(\underline{p}',s')|J_\mu^{\rm em}|N(\underline{p},s)\right\rangle_{\not{CP}} = \bar{u}_N(\underline{p}',s')\Gamma_\mu^{\not{CP}}(q^2)u_N(\underline{p},s)\,, \tag{7}$$

where $J_\mu^{\rm em}$ is the electromagnetic current, and $\underline{p}\,(\underline{p}')$ and $s\,(s')$ represent the nucleon momentum and spin, respectively. For a small CP-violating coupling $\tilde{g}$ (e.g., $\bar{\theta}$ in the case of the theta term), the matrix element can be expressed in terms of CP-even form factors $F_1(q^2)$ and $F_2(q^2)$, and the CP-odd form factor $F_3(q^2)$

$$\Gamma_\mu^{\not{CP}}(q^2) = F_1(q^2)\gamma_\mu + \frac{i}{2M_{\rm N}}F_2(q^2)\sigma_{\mu\nu}q_\nu + \tilde{g}\frac{i}{2M_{\rm N}}F_3(q^2)\sigma_{\mu\nu}\gamma_5 q_\nu\,. \tag{8}$$

The nucleon EDM is extracted from the CP-odd form factor $F_3(q^2)$ at zero recoil ($q = p' - p$) via the relation $d_{\rm N} = \frac{F_3(0)}{2M_{\rm N}}\tilde{g}$.

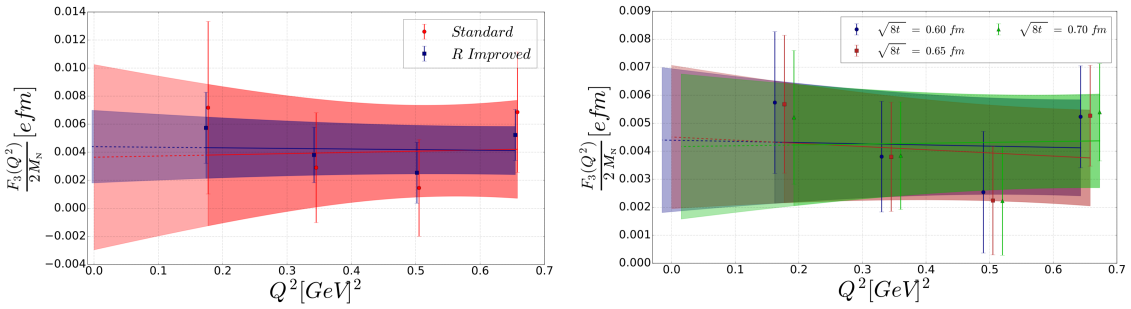

Figure 5: Left: Dependence of the CP-violating form factor $F_3(Q^2)$ on the momentum transfer Q^2, illustrating the difference between correlation functions with (blue data and band) and without (red data and band) signal-to-noise ratio improvements. Right: values of $F_3(Q^2)$ determined for various flow times at which the topological charge is evaluated.

Several approaches are available to compute the matrix element in Eq. (7). These include the background field method [26], and analytical continuation to imaginary CP-odd coupling, as applied to the theta term in Ref. [27]. In the next section, we focus on a perturbative expansion in the CP-odd coupling. This method involves evaluating the three-point function of the electromagnetic current between nucleon interpolators, with the CP-odd operator integrated over the entire space-time volume $L^3 \times T$.

4.1 Electric dipole moment from the θ term

To compute the contribution of the θ term to the nucleon EDM (nucleon θEDM) using lattice QCD, it is essential to have a theoretically and numerically robust definition of the topological charge density. The gradient flow (GF) for gauge fields [28] provides such a definition, offering a well-defined continuum limit while remaining free from ultraviolet (UV) divergences at positive flow time, $t > 0$. Additionally, the topological charge remains independent of the flow time [28, 29], simplifying the evaluation of the θ term contribution. It is sufficient to compute the topological charge at positive flow time and then take the continuum limit of the CP-odd form factor to determine the EDM.

Resolved the UV issues leave the challenge of improving the signal-to-noise ratios of the relevant lattice correlation functions. Various methods have been proposed to address this, most focusing on isolating space-time regions where the signal is exponentially suppressed and discarding these regions to reduce noise in the correlation functions. Examples of these techniques are discussed in Refs. [30–35].

In Ref. [33], a method was developed following similar principles, enabling the determination of CP-odd form factors. The left plot in Fig. 5 illustrates the Q^2 dependence of the CP-odd form factor, shown both before and after signal-to-noise improvement. The right plot demonstrates the expected flow-time independence within the hadronic region, 0.6 fm $< \sqrt{8t} <$ 0.7 fm.

A study of the pion mass dependence has given a nEDM of $d_n = -0.00152(71)\ \theta\ e$ fm. Combined with current experimental bounds, this result constrains the θ parameter to $|\theta| < 1.98 \times 10^{-10}$ at 90% confidence level. Furthermore, the pion mass dependence of the nEDM provides an estimate for the CP-odd coupling, $\overline{g}_0^\theta = -1.28(64) \cdot 10^{-1}\ \theta$. This value agrees well with an

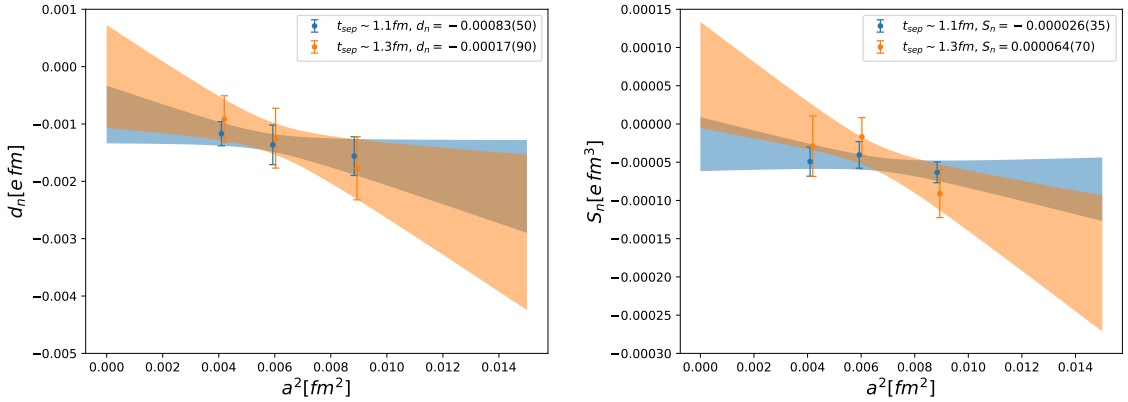

Figure 6: Continuum limit of the nEDM (left plot) and the neutron Schiff moment (right plot) both induced by the θ term. Different colors represent different physical separation, $t_{\rm sep}$, between the nucleon interpolators.

independent determination [36] based on lattice QCD calculations of neutron-proton mass splitting from QCD isospin breaking effects, $\overline{g}_0^\theta = -1.47(23) \cdot 10^{-1}\ \theta$. The consistency of these results reinforces the reliability of the nEDM estimates and the pion mass dependence analysis.

Major systematics of this calculation are the study of lighter pion masses closer to the physical point and the increased excited states contamination (ESC). To perform a step forward in this direction and have a robust study of the continuum limit we are extending this calculation using OpenLat gauge configurations [37–40]. The Open Lattice Initiative[2] (OpenLat) is an effort aimed at generating large-scale gauge ensembles for broad use within the scientific community. Currently, OpenLat focuses on producing gauge ensembles with $N_f = 2 + 1$ flavors of Wilson fermions, following a detailed and systematic plan [40]. All computations are conducted within the stabilized Wilson fermion (SWF) framework [41], which employs the Lüscher-Weisz improved gauge action [42, 43], and the exponentiated Clover action for quarks [41], with the clover coefficient tuned non-perturbatively [37, 41].

Since this study aims to provide a robust estimate of systematic uncertainties, we proceed incrementally. The first step focuses on the continuum limit in the unphysical scenario where the three light quarks are degenerate, corresponding to a pseudoscalar mass of $m_\pi \simeq 411$ MeV.

The plots in Fig. 6 present preliminary results obtained on OpenLat gauge configurations. The left plot illustrates the continuum limit of the nEDM, with different colors representing results for source-sink separations of $t_{\rm sep} \simeq 1.1$ fm and $t_{\rm sep} \simeq 1.3$ fm. Similarly, the right plot shows the continuum limit of the Schiff moment[3] for the same source-sink separations. It is important to emphasize that these results are very preliminary and a more quantitative discussion should follow after a more final data analysis. A cursory look at the results in Fig. 6 indicate that if there are ESC they are below the current statistical uncertainties, but adopting the large source-sink separation data set we reach a vanishing neutron EDM in the continuum limit. Clearly a larger statistics and more values of source-sink separation are necessary to finalize this calculation.

Recent years have seen significant progress in neutron θEDM calculations. The ETM Collab-

[2]https://openlat1.gitlab.io

[3]The Schiff moment here corresponds to the normalized slope in Q^2 of the CP-odd form factor $F_3(Q^2)$ at $Q^2 = 0$.

oration presented results [44] using $N_f = 2+1+1$ dynamical quarks at physical light quark masses and a single lattice spacing $a \simeq 0.08$ fm, yielding $|d_n| = 0.0009(24)\ \bar{\theta}\ e$ fm. An important aspect of this work is the use of the topological charge defined through spectral projectors, providing a complementary approach to the GF for better control of the continuum limit.

The Los Alamos National Laboratory (LANL) group conducted a comprehensive study of the neutron θEDM, carefully addressing lattice spacing and pion mass effects [34]. A key observation was the potential systematic uncertainty arising from differences in constraining ESCs through $N\pi$ contributions versus relying solely on LQCD data.

The χQCD Collaboration recently published results using HYP-smeared Domain Wall sea quarks and Overlap valence quarks at $a \simeq 0.11$ fm [35]. Their approach employed a topological charge definition based on the Overlap lattice Dirac propagator, leading to a neutron EDM result of $d_n = -0.00148(14)(31)\ \bar{\theta}\ e$ fm. These studies highlight the need for improvements in critical areas. Enhancing signal-to-noise ratios, either through two orders of magnitude higher statistics or advanced methodologies, is essential. A deeper understanding of ESC effects, particularly near physical light quark masses, is required. Reducing statistical uncertainties is crucial for effectively analyzing lattice correlation functions. Additionally, discretization effects and continuum extrapolations demand more attention. Both ETMC and χQCD results are limited to single lattice spacings, with the former being obtained at the physical point. SymLat and LANL analyses, on the other hand, include global fits that account for lattice spacing and pion mass dependence. However, neither single lattice spacing results nor global fits sufficiently address the continuum limit, underscoring the need for more comprehensive studies with finer lattice spacings and improved methodologies. Expanding the ensemble set to include multiple quark masses and lattice spacings smaller than ~ 0.1 fm is necessary to resolve systematic uncertainties.

If the next generation of θEDM calculations, expected in 3-5 years, wants to achieve more precise constraints on the θ-term contribution to EDMs and deepen our understanding of CP violation, it must address these challenges comprehensively.

5. BSM operators and the gradient flow

At the hadronic scale, BSM contributions to the EDMs are characterized by CP-odd operators of dimensions higher than four. The qCEDM, introduced in Eq. (4), is a dimension-5 operator that contributes to the neutron EDM and other systems. While the challenges of the neutron θEDM largely come from the degradation of the signal-to-noise ratio (SNR) in the chiral and infinite volume limits, the qCEDM faces an additional obstacle: its complex renormalization pattern. It has been shown in Ref. [45] the renormalization of the qCEDM using MOM-type of schemes results in a large number of operator mixing basis that increase when using Wilson-type fermions. Moreover, unavoidable power divergences proportional to $1/a^2$ persist, even with Ginsparg-Wilson lattice actions, due to mixing between operators of the same chirality.

For the qCEDM, the GF offers a promising approach by improving the renormalization properties of local operators at finite flow time [46–51]. This enables better control over the otherwise challenging renormalization process associated with the qCEDM. An alternative method to control the power divergences, based on an axial Ward identity, has been proposed in Ref. [52].

The connection between operators renormalized at finite flow time and those at $t = 0$ in QCD can be established through perturbative methods in the continuum [53–60]. In this framework, the short flow-time expansion (SFTX) provides a systematic method to match finite flow-time operators to their QCD counterparts. Non-perturbative methods relying on Ward identities [61–63] provide an alternative approach, independent of perturbative expansions.

The strategy for the computation of BSM contributions to the EDMs can be summarize in few steps. First, one computes the relevant hadronic matrix element of the flowed operator. Second, after renormalizing the flowed quark fields one performs the continuum limit at fixed flow time. Third, one matches the results at finite flow times with the results in the $\overline{\text{MS}}$ scheme using the matching coefficients obtained in perturbative QCD in the context of the SFTX. The renormalization of flowed local fields is very simple and amounts to renormalize the flowed quark fields, thus any bilinear renormalizes in the same way with a factor $Z_\chi^{1/2}$ for each quark field. This implies that ratios of flowed bilinears are free of ultraviolet divergences. A practical scheme to renormalize flowed quark fields is to define *ringed* fields [53], , denoted as $\mathring{\chi}$ and $\overline{\mathring{\chi}}$, and defined by the gauge-invariant condition $\left\langle \overline{\mathring{\chi}}(x,t)\overleftrightarrow{\not{D}}\mathring{\chi}(x,t)\right\rangle = -\frac{N_c}{(4\pi)^2 t^2}$. This condition provides a significant advantage due to its regularization independence, making it applicable both in perturbative frameworks and non-perturbative lattice QCD simulations. Alternatively it is possible to study ratios of flowed matrix elements and then perform the matching of such ratios. An important annotation in this method is the case when flowed fields receive contributions from lower dimensional fields in the SFTX. This is the case for the qCEDM and the gCEDM discussed here. At small flow times, the flowed qCEDM receives contribution from the pseudoscalar density with a coefficient proportional to $1/t$. In such cases, the power-divergent term cannot be subtracted using a coefficient determined in perturbation theory, as this would introduce uncontrolled systematic uncertainties due to power-divergent neglected higher-order corrections.

The strategy we have proposed for the qCEDM can be summarized as follows, where for simplicity we omit flavor indices. The SFTX of the qCEDM operator defined with ringed fields

$$\mathring{O}_{\text{qC}}(t) = \overline{\mathring{\chi}}(t)\gamma_5\sigma_{\mu\nu}G_{\mu\nu}(t)\mathring{\chi}(t)\,, \tag{9}$$

is given by

$$\mathring{O}_{\text{qC}}(t) = \frac{c_{\text{OP}}(t,\mu)}{t}P_{\text{R}}(0,\mu) + \sum_i c_{\text{qC},i}(t,\mu)O_{i,\text{R}}(0,\mu) + O(t)\,, \tag{10}$$

where we indicate with $O_{i,\text{R}}$ generically the dimension = 5 operators contributing to the SFTX, including our target operator of the qCEDM at vanishing flow time, $O_{\text{qC,R}}$. The renormalized operators are assumed renormalized in the same scheme adopted to determine the matching coefficients, $c_{\text{qC},i}$. The coefficient of the power divergent term can then be defined from the ratio

$$t\frac{\left\langle \mathring{O}_{\text{qC}}(t)P(0)\right\rangle}{\langle P_{\text{R}}(0,\mu)P(0)\rangle} = t\frac{\langle O_{\text{qC}}(t)P(0)\rangle}{\langle P(t)P(0)\rangle}\frac{\left\langle \mathring{P}(t)P(0)\right\rangle}{\langle P_{\text{R}}(0,\mu)P(0)\rangle} = \Delta(\bar{g}^2)\Delta_P(t,\mu) \tag{11}$$

where

$$\Delta(\bar{g}^2) = t\frac{\left\langle O_{\text{qC}}(t)P(0)\right\rangle}{\langle P(t)P(0)\rangle}\,, \quad \text{and} \quad \Delta_P(t,\mu) = \frac{\left\langle \mathring{P}(t)P(0)\right\rangle}{\langle P_{\text{R}}(0,\mu)P(0)\rangle}\,. \tag{12}$$

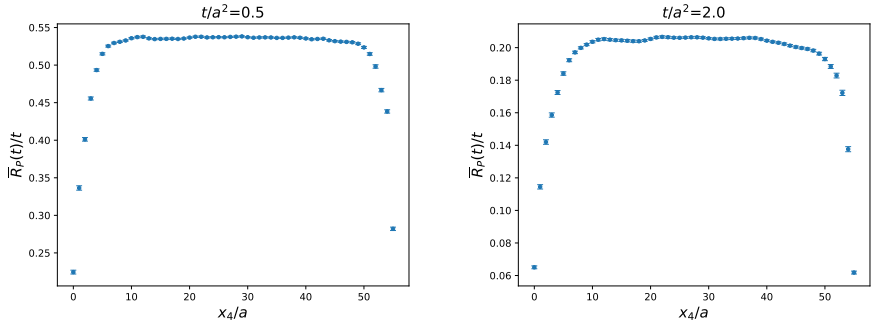

Figure 7: Dependence of the ratio of correlation functions, $\frac{\Gamma_{\rm CP}(x_4;t)}{\Gamma_{\rm PP}(x_4;t)}$, on Euclidean time x_4/a, shown for two flow times: $t/a^2 = 0.5$ and $t/a^2 = 2.0$

The O(t) terms affecting the determination of $c_{\rm OP}(t,\mu)$

$$c_{\rm OP}(t,\mu) = \Delta(\bar{g}^2)\Delta_{\rm P}(t,\mu) + O(t) \tag{13}$$

have to be considered carefully when subtracting the power divergence to determine the physical matrix element.

The SFTX of a generic matrix element of the qCEDM denoted as $\left\langle \mathring{O}_{\rm qC}(t)\Phi \right\rangle$, is given by

$$\left\langle \mathring{O}_{\rm qC}(t)\Phi \right\rangle = \frac{1}{t}\Delta(\bar{g}^2)\Delta_P(t,\mu)\left\langle P_{\rm R}(0,\mu)\Phi\right\rangle + F\left[c_{{\rm qC},i}(t,\mu), \left\langle P_{\rm R}(0,\mu)\Phi\right\rangle, \left\langle O_{i,{\rm R}}(0,\mu)\Phi\right\rangle\right], \tag{14}$$

where with $F[]$ we denote a function of the correlators and coefficients that appear in the argument. One has all the ingredients needed to a determination of the renormalized qCEDM matrix element at $t = 0$, related to $\left\langle O_{\rm qC,R}(0,\mu)\Phi\right\rangle$. In Ref. [49] we have performed a first study of the power divergence. We have studied the finite renormalization $\Delta(\bar{g}^2)$ and compared the results with perturbative QCD [48, 50]. We have defined $\Delta(\bar{g}^2)$ non perturbatively using the ratio

$$\overline{R}_{\rm P}(x_4;t) = t\frac{\Gamma_{\rm CP}(x_4;t)}{\Gamma_{\rm PP}(x_4,t)}, \tag{15}$$

where

$$\Gamma_{CP}(x_4;t) = a^3\sum_{\mathbf{x}}\left\langle O_{\rm qC}(x_4,\mathbf{x};t)P(0,\mathbf{0};0)\right\rangle, \quad \Gamma_{PP}(x_4;t) = a^3\sum_{\mathbf{x}}\left\langle P(x_4,\mathbf{x};t)P(0,\mathbf{0})\right\rangle, \tag{16}$$

where for simplicity, we omit flavor indices. However, the interpolators in the correlator should be understood as involving flowed fermion fields of different flavors, thereby excluding disconnected diagrams. The plots in Fig. 7 show the plateau values, for 2 values of the flow time, for large x_4 of $\overline{R}_{\rm P}(x_4;t)$, corresponding to the vacuum-to-pion hadronic matrix element. This provides a non-perturbative definition of $\Delta(\bar{g}^2)$ with a finite continuum limit. Fig. 8 presents the raw lattice data together with the determination of $\Delta(\bar{g}^2)$ after performing the chiral and continuum extrapolations. The left plot shows a polynomial representation as a function of the renormalized coupling $\bar{g}^2$, up to order $\bar{g}^8$, while the right plot shows a polynomial constrained at leading order, O($\bar{g}^2$), using the perturbative result [48, 50], depicted as a straight green line. Although these results require

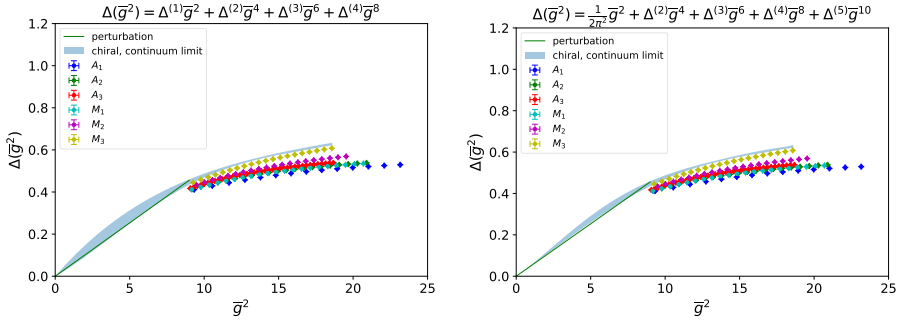

Figure 8: Dependence of the function $\Delta(\overline{g}^2)$ on the strong coupling $\overline{g}$. The left plot shows a polynomial fit up to $\overline{g}^8$, derived from lattice data after continuum and chiral extrapolation. The right plot extends the polynomial fit to $\overline{g}^{10}$, with the leading $O(\overline{g}^2)$ term constrained by perturbative QCD results [48], indicated by the green straight line.

validation with state-of-the-art gauge configurations, they demonstrate the feasibility of determining the finite renormalization that connects higher-dimensional operators to lower-dimensional ones over a wide range of renormalized couplings. A complete non-perturbative subtraction of the power divergence in the physical matrix element still depends on a non-perturbative determination of the matching coefficient for the pseudoscalar density, which is currently underway.

To determine the flow-time dependent coefficients $c_{\mathrm{qC},i}(t,\mu)$, we evaluate the insertion of the operators $O_{\mathrm{qC}}(t)$ within off-shell amputated one-particle irreducible (1PI) Green's functions. These are matched with its SFTX containing all the operators O_i at $t = 0$, probed with unflowed fermion and gauge fields. The calculations are performed in the massless limit, with matching conducted to one-loop accuracy. Explicitly incorporating the quark mass terms into the operators ensures that the one-loop coefficients $c^{(1)}_{\mathrm{qC},i}(t,\mu)$ remain independent of the low-energy scales.

After renormalizing in a given scheme the strong coupling, let us say for definiteness the $\overline{\mathrm{MS}}$ scheme, we normalize the flowed fermion fields (e.g., using ringed fields). Standard matching techniques [64–66] can be applied, where the loop integrands are expanded in all scales except the flow time t prior to integration. Although this expansion modifies the infrared (IR) structures of the loop integrals, the IR alterations cancel in the difference between the $\overline{\mathrm{MS}}$ and flowed diagrams.

Expanding the loop integrals results in scaleless integrals for operator insertions on the $t = 0$ side of the matching equations, which vanish in dimensional regularization. As a result, the ultraviolet (UV) and IR singularities of the expanded loops remain identical. Flowed operator insertions are inherently free of UV singularities, aside from the gauge coupling renormalization and the quark-field renormalization factor $Z_\chi^{1/2}$. The IR singularities from the expanded loop integrals on the flowed, $t > 0$, side of the matching equations, match the UV $\overline{\mathrm{MS}}$ counterterms exactly.

The finite matching coefficients $c_{\mathrm{qC},i}$ are then straightforward to compute using the expanded integrals of flowed operator insertions, which reduce to single-scale integrals. Even with the inclusion of general gauge parameters, the calculations remain manageable. Performing computations with generic gauge parameters provides a robust check, as the coefficients $c_{\mathrm{qC},i}$ of gauge-invariant operators in the SFTX must be independent of these parameters.

The list of Feynman diagrams needed to compute the matching coefficient $c_{\mathrm{qC,qC}}$ are depicted in Fig. 9. Beside the standard Feynman diagrams there are additional Feynman diagrams coming from the perturbative expansion of the GF equation (depicted in the red box). Feynman rules can be found for example in Refs. [48, 50]. As an example of resulting matching coefficient I report here at next-to-leading order (NLO)

$$c_{\mathrm{qC,qC}}(t,\mu) = 1+\frac{\alpha_s}{4\pi}\left[(5C_F-2C_A)\log(8\pi\mu^2 t)-\frac{1}{2}\Big((4+5\delta_{\mathrm{HV}})C_A+(3-4\delta_{\mathrm{HV}})C_F\Big)-\log(432)C_F\right], \quad (17)$$

where $C_F = 4/3$, and $C_A = 3$ in QCD. The parameter δ_{HV} takes value 0 or 1 resepctively in the scheme with anticommuting γ_5 or in the 't Hooft-Veltman scheme [67]. The extension of this calculation to next-to-next-to-leading order (NNLO) is ongoing [51] using the tools introduced in Ref. [59].

A similar calculation has been performed in [68] for the gCEDM operator defined in Eq. (5). As an example of result in the MS scheme for the matching of the gCEDM into itself is given by

$$c_{\mathrm{gC,gC}} = 1 + \frac{\alpha_s}{4\pi}\left[6C_A\log(8\pi\mu^2 t) + \frac{C_A}{3}\right], \quad (18)$$

6. Summary and Outlook

Detecting an electric dipole moment (EDM) in systems such as neutrons, atoms, or molecules at current sensitivities would mark a significant breakthrough in physics, probing Beyond the Standard Model (BSM) at mass scales beyond those accessible to colliders. However, a single EDM measurement cannot distinguish between BSM theories or clarify the nature of CP-violation. A coordinated program across atomic, molecular, nuclear, and particle physics is essential to address these questions.

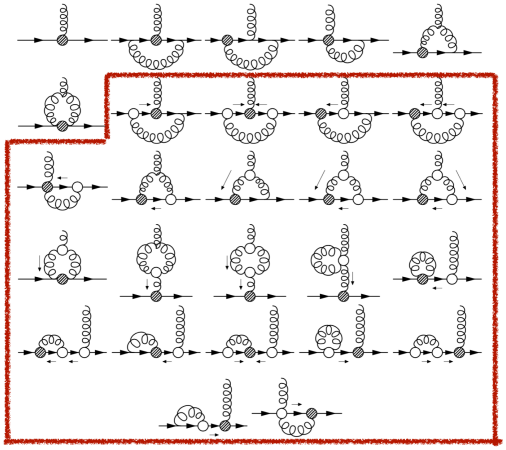

Figure 9: Feynman diagrams illustrating the contributions to the matching coefficient of the qCEDM into itself at vanishing flow time. The diagrams enclosed in the red boxed area represent new contributions arising from the perturbative expansion of the GF equations.

Effective field theory describes low-energy effects of BSM physics through quark and gluon operator matrix elements. Estimating these matrix elements requires non-perturbative techniques due to the strong coupling at relevant scales. While methods like dimensional analysis, sum rules, and chiral effective field theory provide approximate estimates, their accuracy is limited by uncontrolled approximations. Recent advancements in lattice QCD (LQCD) offer more reliable matrix element calculations with well-defined uncertainties.

First LQCD calculations of the hadronic matrix elements relevant for EDMs are beginning to provide reliable estimates, despite the significant challenges they face. The nucleon EDM induced

by the θ term continues to suffer from severe signal-to-noise issues, but recent results have started to show signals significantly different from zero. Although we are not yet in the precision era for these calculations, ongoing efforts to critically assess and address remaining systematic uncertainties are paving the way for more robust and impactful results. To make sure the next generation of LQCD calculations for the θEDM are impactful for upcoming experiments, a substantial increase in simulation statistics or the development of more effective noise reduction techniques will be essential; however, if the signal is particularly small, even such improvements may not be sufficient. Additionally, systematic uncertainties from excited state contamination and discretization effects must be carefully controlled to ensure the results are meaningful.

The renormalization of the BSM operators has long been a major obstacle to a reliable determination, using LQCD, of the BSM contributions to the nucleon EDMs. Recently new techniques based on the gradient flow have shown potentials to resolve the renormalization challenge, and already several results in perturbative QCD and LQCD have been obtained. All the technical and theoretical advancements of the past few years should finally see applications in the next 5 years, where we should see more precise results for the θEDM and first results for some BSM contributions to the nucleon EDMs.

Acknowledgments

I have profited from discussions about the electric dipole moment and the gradient flow with Vincenzo Cirigliano, Skyler Degenkolb, Jordy de Vries, Jack Dragos, Robert Harlander, Anna Hasenfratz, Jangho Kim, Keh-Fei Liu, Tom Luu, Emanuele Mereghetti, Christopher J. Monahan, Matthew D. Rizik, Jaideep Singh, Peter Stoffer, Andre Walker-Loud and Oliver Witzel. I want to thank the OpenLat members Francesca Cuteri, Anthony Francis, Patrick Fritzsch, Jangho Kim, Giovanni Pederiva, Dimitra A. Pefkou, Antonio Rago, Andre Walker-Loud and Savvas Zafeiropoulos for a most enjoyable collaboration. I especially want to thank Jangho Kim for helping with plots and analysis presented in Sec. 2.1. I acknowledge funding support from Deutsche Forschungsgemeinschaft (DFG, German Research Foundation) through grant 513989149, from the National Science Foundation grant PHY-2209185 and from the DOE Topical Collaboration Nuclear Theory for New Physics award No. DE-SC0023663. Numerical calculations for some of the results presented in this contributions were performed using resources from the National Energy Research Scientific Computing Center (NERSC), a Department of Energy Office of Science User Facility, under NERSC award NP-ERCAP0027662; and the Gauss Centre for Supercomputing e.V. (www.gauss-centre.eu) on the GCS Supercomputer JUWELS [69] at the Jülich Supercomputing Centre (JSC). I also acknowledge the EuroHPC Joint Undertaking for awarding this project access to the EuroHPC supercomputer LEONARDO, hosted by CINECA (Italy) and LUMI at CSC (Finland). The author acknowledges support as well as computing and storage resources by GENCI on Adastra and Occigen (CINES), Jean-Zay (IDRIS) and Irène-Joliot-Curie (TGCC) under projects (2020-2024)-A0080511504 and (2020-2024)-A0080502271 through which gauge generation for the Openlat collaboration has been made possible.

References

[1] S. Navas *et al.* [Particle Data Group], Phys. Rev. D **110**, 030001 (2024).

[2] T.-H. Yeh, J. Shelton, K. A. Olive, and B. D. Fields, JCAP **10**, 046 (2022), [arXiv:2207.13133 [astro-ph.CO]].

[3] R. J. Cooke, M. Pettini, and C. C. Steidel, Astrophys. J. **855**, 102 (2018), [arXiv:1710.11129 [astro-ph.CO]].

[4] G. Jungman, M. Kamionkowski, A. Kosowsky, and D. N. Spergel, Phys. Rev. D **54**, 1332 (1996), [arXiv:astro-ph/9512139].

[5] N. Aghanim *et al.* [Planck Collaboration], Astron. Astrophys. **641**, A6 (2020), [arXiv:1807.06209 [astro-ph.CO]], [Erratum: Astron.Astrophys. 652, C4 (2021)].

[6] A. Sakharov, Sov. Phys. Usp. **34**, 392 (1991).

[7] N. Cabibbo, Phys. Rev. Lett. **10**, 531 (1963).

[8] M. Kobayashi and T. Maskawa, Prog. Theor. Phys. **49**, 652 (1973).

[9] M. Shaposhnikov, Nucl. Phys. B **287**, 757 (1987).

[10] M. Gavela, P. Hernandez, J. Orloff, and O. Pene, Mod. Phys. Lett. A **9**, 795 (1994), [arXiv:hep-ph/9312215].

[11] P. Huet and E. Sather, Phys. Rev. D **51**, 379 (1995), [arXiv:hep-ph/9404302].

[12] A. G. Cohen, D. Kaplan, and A. Nelson, Ann. Rev. Nucl. Part. Sci. **43**, 27 (1993), [arXiv:hep-ph/9302210].

[13] E. Salpeter, Phys. Rev. **112**, 1642 (1958).

[14] R. Alarcon *et al.*, "Electric dipole moments and the search for new physics," in *Snowmass 2021*. 3, 2022. arXiv:2203.08103 [hep-ph].

[15] C. Abel *et al.* [nEDM Collaboration], Phys. Rev. Lett. **124**, 081803 (2020), [arXiv:2001.11966 [hep-ex]].

[16] A. P. Serebrov *et al.*, Phys. Rev. C **92**, 055501 (2015).

[17] D. Wurm *et al.*, EPJ Web Conf. **219**, 02006 (2019), [arXiv:1911.09161 [physics.ins-det]].

[18] J. W. Martin, J. Phys. Conf. Ser. **1643**, 012002 (2020).

[19] T. Ito *et al.*, Phys. Rev. C **97**, 012501 (2018), [arXiv:1710.05182 [physics.ins-det]].

[20] E. Shabalin, Sov. J. Nucl. Phys. **28**, 75 (1978).

[21] E. Shabalin, Sov. Phys. Usp. **26**, 297 (1983).

[22] C.-Y. Seng, Phys. Rev. **C91**, 025502 (2015), [arXiv:1411.1476 [hep-ph]].

[23] V. Cirigliano and M. J. Ramsey-Musolf, Prog. Part. Nucl. Phys. **71**, 2 (2013), [arXiv:1304.0017 [hep-ph]].

[24] J. de Vries, P. Draper, K. Fuyuto, J. Kozaczuk, and B. Lillard, Phys. Rev. D **104**, 055039 (2021), [arXiv:2107.04046 [hep-ph]].

[25] K.-F. Liu, [arXiv:2411.15198 [hep-lat]].

[26] F. He, M. Abramczyk, T. Blum, T. Izubuchi, H. Ohki, and S. Syritsyn, PoS **LATTICE2023**, 336 (2024), [arXiv:2311.06106 [hep-lat]].

[27] F. K. Guo, R. Horsley, U.-G. Meißner, Y. Nakamura, H. Perlt, P. E. L. Rakow, G. Schierholz, A. Schiller, and J. M. Zanotti, Phys. Rev. Lett. **115**, 062001 (2015), [arXiv:1502.02295 [hep-lat]].

[28] Lüscher, M., JHEP **1008**, 071 (2010), [arXiv:1006.4518 [hep-lat]].

[29] M. Cè, C. Consonni, G. P. Engel, and L. Giusti, Phys. Rev. **D92**, 074502 (2015), [arXiv:1506.06052 [hep-lat]].

[30] E. Shintani, T. Blum, T. Izubuchi, and A. Soni, Phys. Rev. **D93**, 094503 (2016), [arXiv:1512.00566 [hep-lat]].

[31] K.-F. Liu, J. Liang, and Y.-B. Yang, Phys. Rev. D **97**, 034507 (2018), [arXiv:1705.06358 [hep-lat]].

[32] S. Syritsyn, T. Izubuchi, and H. Ohki, PoS **Confinement2018**, 194 (2019), [arXiv:1901.05455 [hep-lat]].

[33] J. Dragos, T. Luu, A. Shindler, J. de Vries, and A. Yousif, Phys. Rev. C **103**, 015202 (2021), [arXiv:1902.03254 [hep-lat]].

[34] T. Bhattacharya, V. Cirigliano, R. Gupta, E. Mereghetti, and B. Yoon, Phys. Rev. D **103**, 114507 (2021), [arXiv:2101.07230 [hep-lat]].

[35] J. Liang, A. Alexandru, T. Draper, K.-F. Liu, B. Wang, G. Wang, and Y.-B. Yang [χQCD Collaboration], Phys. Rev. D **108**, 094512 (2023), [arXiv:2301.04331 [hep-lat]].

[36] J. de Vries, E. Mereghetti, and A. Walker-Loud, Phys. Rev. **C92**, 045201 (2015), [arXiv:1506.06247 [nucl-th]].

[37] A. S. Francis, F. Cuteri, P. Fritzsch, G. Pederiva, A. Rago, A. Shindler, A. Walker-Loud, and S. Zafeiropoulos, PoS **LATTICE2021**, 118 (2022), [arXiv:2201.03874 [hep-lat]].

[38] F. Cuteri, A. S. Francis, P. Fritzsch, G. Pederiva, A. Rago, A. Shindler, A. Walker-Loud, and S. Zafeiropoulos, PoS **LATTICE2022**, 426 (2023), [arXiv:2212.07314 [hep-lat]].

[39] F. Cuteri, A. Francis, P. Fritzsch, G. Pederiva, A. Rago, A. Shindler, A. Walker-Loud, and S. Zafeiropoulos, PoS **LATTICE2022**, 074 (2023), [arXiv:2212.11048 [hep-lat]].

[40] A. Francis, F. Cuteri, P. Fritzsch, G. Pederiva, A. Rago, A. Shindler, A. Walker-Loud, and S. Zafeiropoulos, PoS **LATTICE2023**, 048 (2024), [arXiv:2312.11298 [hep-lat]].

[41] A. Francis, P. Fritzsch, M. Lüscher, and A. Rago, Comput. Phys. Commun. **255**, 107355 (2020), [arXiv:1911.04533 [hep-lat]].

[42] M. Luscher and P. Weisz, Commun. Math. Phys. **98**, 433 (1985), [Erratum: Commun.Math.Phys. 98, 433 (1985)].

[43] M. Luscher and P. Weisz, Phys. Lett. B **158**, 250 (1985).

[44] C. Alexandrou, A. Athenodorou, K. Hadjiyiannakou, and A. Todaro, Phys. Rev. D **103**, 054501 (2021), [arXiv:2011.01084 [hep-lat]].

[45] T. Bhattacharya, V. Cirigliano, R. Gupta, E. Mereghetti, and B. Yoon, Phys. Rev. **D92**, 114026 (2015), [arXiv:1502.07325 [hep-ph]].

[46] A. Shindler, J. de Vries, and T. Luu, PoS **LATTICE2014**, 251 (2014), [arXiv:1409.2735 [hep-lat]].

[47] J. Kim, J. Dragos, A. Shindler, T. Luu, and J. de Vries, "Towards a determination of the nucleon EDM from the quark chromo-EDM operator with the gradient flow," in *36th International Symposium on Lattice Field Theory (Lattice 2018) East Lansing, MI, United States, July 22-28, 2018*. 2018. arXiv:1810.10301 [hep-lat].

[48] M. D. Rizik, C. J. Monahan, and A. Shindler [SymLat Collaboration], Phys. Rev. D **102**, 034509 (2020), [arXiv:2005.04199 [hep-lat]].

[49] J. Kim, T. Luu, M. D. Rizik, and A. Shindler [SymLat Collaboration], Phys. Rev. D **104**, 074516 (2021), [arXiv:2106.07633 [hep-lat]].

[50] E. Mereghetti, C. J. Monahan, M. D. Rizik, A. Shindler, and P. Stoffer, JHEP **04**, 050 (2022), [arXiv:2111.11449 [hep-lat]].

[51] R. Harlander, M. D. Rizik, J. Borgulat, and A. Shindler, PoS **LATTICE2022**, 313 (2023), [arXiv:2212.09824 [hep-lat]].

[52] T. Bhattacharya, V. Cirigliano, R. Gupta, E. Mereghetti, J.-S. Yoo, and B. Yoon, Phys. Rev. D **108**, 074507 (2023), [arXiv:2304.09929 [hep-lat]].

[53] H. Makino and H. Suzuki, PTEP **2014**, 063B02 (2014), [arXiv:1403.4772 [hep-lat]].

[54] T. Endo, K. Hieda, D. Miura, and H. Suzuki, PTEP **2015**, 053B03 (2015), [arXiv:1502.01809 [hep-lat]].

[55] K. Hieda and H. Suzuki, Mod. Phys. Lett. **A31**, 1650214 (2016), [arXiv:1606.04193 [hep-lat]].

[56] R. V. Harlander and T. Neumann, JHEP **06**, 161 (2016), [arXiv:1606.03756 [hep-ph]].

[57] C. Monahan, Phys. Rev. **D97**, 054507 (2018), [arXiv:1710.04607 [hep-lat]].

[58] R. V. Harlander, Y. Kluth, and F. Lange, Eur. Phys. J. **C78**, 944 (2018), [arXiv:1808.09837 [hep-lat]], [Erratum: Eur. Phys. J.C79,no.10,858(2019)].

[59] J. Artz, R. V. Harlander, F. Lange, T. Neumann, and M. Prausa, JHEP **06**, 121 (2019), [arXiv:1905.00882 [hep-lat]], [Erratum: JHEP 10, 032 (2019)].

[60] A. Suzuki, Y. Taniguchi, H. Suzuki, and K. Kanaya, Phys. Rev. D **102**, 034508 (2020), [arXiv:2006.06999 [hep-lat]].

[61] L. Del Debbio, A. Patella, and A. Rago, JHEP **11**, 212 (2013), [arXiv:1306.1173 [hep-th]].

[62] Lüscher, M., JHEP **1304**, 123 (2013), [arXiv:1302.5246 [hep-lat]].

[63] A. Shindler, Nucl.Phys. **B881**, 71 (2014), [arXiv:1312.4908 [hep-lat]].

[64] A. V. Manohar, Lect. Notes Phys. **479**, 311 (1997), [arXiv:hep-ph/9606222].

[65] A. V. Manohar, Phys. Rev. D **56**, 230 (1997), [arXiv:hep-ph/9701294].

[66] A. V. Manohar, [arXiv:1804.05863 [hep-ph]].

[67] G. 't Hooft and M. Veltman, Nucl. Phys. B **44**, 189 (1972).

[68] O. L. Crosas, C. J. Monahan, M. D. Rizik, A. Shindler, and P. Stoffer, Phys. Lett. B **847**, 138301 (2023), [arXiv:2308.16221 [hep-lat]].

[69] Jülich Supercomputing Centre, Journal of Large-Scale Research Facilities **7**, A183 (2021).